# Gas phase detection of Chemical Warfare Agents CWAs with portable Raman

Marta Lafuente [a,b], Diego Sanz [a,b], Miguel Urbiztondo [c], Jesús Santamaría [a,b,d] María Pilar Pina [a,b,d], Reyes Mallada [a,b,d,*]

[a]Nanoscience Institute of Aragon (INA), University of Zaragoza, Department of Chemical & Environmental Engineering, Edificio I+D+i, Campus Rio Ebro, C/Mariano Esquillor s/n, 50018 Zaragoza, Spain
[b]Instituto de Ciencia de Materiales de Aragón (ICMA), Universidad de Zaragoza-CSIC, 50009 Zaragoza, Spain.
[c]Centro Universitario de la Defensa de Zaragoza, Carretera Huesca s/n, 50090 Zaragoza, Spain.
[d]Networking Research Center on Bioengineering, Biomaterials and Nanomedicine, CIBER-BBN, 28029 Madrid, Spain.
* Corresponding author. Tel: +34 876 555 440; *E-mail address:* rmallada@unizar.es (R.M.)

## Abstract

The development of SERS substrates for chemical detection of specific analytes requires appropriate selection of plasmonic metal and the surface where it is deposited. Here we deposited Ag nanoplates on three substrates: i) conventional $SiO_2$/Si wafer, ii) stainless steel mesh and iii) graphite foils. The SERS enhancement of the signal was studied for Rhodamine 6G (R6G) as common liquid phase probe molecule. We conducted a comprehensive study with λ=532, 633 and 785 nm on all the substrates. The best substrate was investigated, at the optimum laser 785 nm, for gas phase detection of dimethyl methyl phosphonate (DMMP), simulant of the G-series nerve agents, at a concentration of 2.5 ppmV (14 mg/m$^3$). The spectral fingerprint was clearly observed; with variations on the relative intensities of SERS Raman bands compared to bulk DMMP in liquid phase reflects the DMMP-Ag interactions. These interactions were simulated by Density Functional Theory (DFT) calculations and the simulated spectra matched with the experimental one. Finally, we were detected the characteristics DMMP fingerprint with hand-held portable equipment. These results open the way for the application of SERS technique on real scenarios where robust, light-weight, miniaturized and simple to use and cost-effective tools are required by first responders.

**Keywords:** Gas phase detection, SERS, portable Raman, CWAs, trace level

# 1. Introduction

The nerve gas attacks with sarin in Matsumoto (1994) and Tokyo (1995) and in the armed conflict in Syria (Goutha 2013 and Khan Shaykhun 2017) are recent and representative examples of the present world threat spectrum. Chemical Warfare Agents (CWAs), initially developed in the First World War, include vesicant and blister agents such as phosgene (PD) and mustard gas (HD) and nerve agents, as sarin (GB) and venomous agent X (VX). The nerve agents are highly toxic due to the irreversible binding with the nerve sites responsible for acetylcholinesterase breakdown, a necessary process in neurotransmission. Sarin gas presents the highest toxicity with a IDLH (Immediately Dangerous to Life or Health) of 0.1 $mg \cdot m^{-3}$. These CWAs are able to spread out in the atmosphere, creating a toxic scenario in few seconds. The early detection and identification of these agents in gas phase is essential for the safety of first responders and for the efficient evacuation of threatened public spaces.

Surface Enhanced Raman Spectroscopy (SERS) is a technique capable of label-free ultrasensitive vibrational "fingerprinting", and as such it is recognized as highly interesting method for explosive and chemical threat detection [1]. The technique has also become suitable for on-site detection thanks to the development of portable equipment with adequate spectral resolution (ranging from 7 to $12cm^{-1}$) and low weight (330 to 2450g) at reasonable prices, ca. 10 thousand euros without spectral library. However there are still several challenges to be overcome before this technique can be implemented as "off-the-shelf" solution for CWA detection.

SERS mainly relies on the enhancement of the Raman signal due to the plasmon resonance of a metallic nanostructure. This effect only occurs when the target molecule is in close contact to the metal, and for this reason an interaction i.e. physical or chemical adsorption is required between the molecule and the metal. The magnitude of the enhancement depends on several parameters including composition, size, morphology, topology, surface distribution, and dielectric environment of the metallic nanostructure on substrate surface. Many efforts have been devoted in SERS field for the development of optimum SERS substrates ranging from fancy shapes of nanoparticles with sharp edges to ordered nanostructures whose the shape and spacing was optimized with simulation and then on fabricated in cleanroom. Other key factors

for the highly sensitive detection of molecules include the cross-section of the molecule, its stability, interactions with the SERS substrate and its solid, liquid or gaseous state.

Most of the SERS applications in the open literature refer to the detection in liquid phase and only few reports for gas phase detection at concentrations below 10 ppmV could be found. Van Duyne and coworkers reported the detection of 8 ppmV of benzene thiol on a SERS substrate consisting of well-ordered silica nanospheres coated with a 200 nm thick Ag film [2]. A recyclable surface-enhanced Raman scattering (SERS) substrate, consisting of Ag nanorods coated with an ultrathin $HfO_2$ shell (Ag NRs@$HfO_2$), was able to detect, after 40 minutes exposure, concentrations in the gas phase as low as 20ppb of the molecule 2-Naphthalenethiol (2-NAT). Then substrate was easily regenerated by heating at 250ºC for 25 seconds [3]. The SERS detection of volatile organic compounds (VOCs) biomarkers in human breath, such as acetone in the case of diabetes or hydrogen cyanide in patients with cystic fibrosis, is gaining of importance as non-invasive tool in primary screening diagnosis. The group of Boisen detected 5ppmV of hydrogen cyanide in gas phase [4] and later on *P. aeruginosa* cultures [5]. The term of *plasmonic nose* was recently coined for a SERS substrate that consists on a core-shell structure of Ag nanocubes encapsulated in porous metal organic framework MOF, in particular ZIF-8 [6]. The VOCs adsorbed on the porous layer formed a 3D confinement space for the molecules near the plasmonic structure. In this system 200 ppmV of toluene were detected and the detection limit could be lowered to 50ppb for 2-nitrotoluene, a molecule with higher cross section. Another recent example of low concentration in gas phase was the detection of 10ppmV of benzene. In this case the strategy for decreasing the detection limit involved deep cooling of the SERS substrate down to -80ºC, to promote adsorption and condensation of the molecules [7]. Recently, a 3D porous substrate successfully detected for the first time 0.1 ppmV of $NO_2$ in the gas phase with a hand-held Raman detector [8]. The high surface area employed consisted of a 3D multilayer structure made of Au coated-Ag nanowires (AgNWs) forming lots of random hot spots in the cross points of the fibers. In our laboratory, the detection of 625 ppbV of DMMP, a surrogate molecule of the G-series nerve agents which are of particular concern due to its extreme toxicity and persistence, was recently reported using a substrate consisting of self-assembled AuNPs coated with a citrate layer that acted as an effective trap for the target molecules [9]. The above results illustrate the importance of substrate selection for gas phase using SERS. It must

provide high electromagnetic enhancement (EF), but also chemical affinity towards the target molecule while avoiding band interference with the functional groups responsible for this affinity.

In this work we selected Ag nanoplates as the plasmonic material to be used in DMMP detection in view of four reasons: i) the optical properties of Ag (real and imaginary parts of the dielectric function), that makes this metal the main candidate to get interesting optical effects, including plasmon resonances [10]; ii) the specific interaction of DMMP with Ag through the P-O bond, as already reported in the first study of DMMP detection in roughened Ag electrodes [11]; iii) the electromagnetic field enhancement at the tips and edges of the nanoplates; and finally, iv) the coincidence of the plasmon resonance band of Ag nanoplates with the excitation laser wavelength used for the Raman measurements, 785nm. We have compared the response of the synthesized Ag nanoplates on three different substrates, $SiO_2$/Si, stainless steel mesh and graphite foil. The SERS response was analyzed using Rhodamine (R6G) as probe molecule with lasers of $\lambda$ = 532, 633 and 785 nm. The same substrates were also studied for the detection of 2.5 ppmV of DMMP in gas phase with a benchtop and portable Raman equipments. The interactions of the DMMP molecule with the Ag surface were simulated using Density Functional Theory (DFT) calculations carried out by Gaussian09 quantum chemistry program [12] to explain the relative intensities variation of the characteristic Raman vibrational modes.

## 2. Materials and methods

### *2.1 Materials*

Silver nitrate ($AgNO_3$, 99.9999%), sodium citrate tribasic dehydrate (>99%), hydrogen peroxide solution ($H_2O_2$, 30% wt), potassium bromide (KBr, >99%), sodium borohydride ($NaBH_4$, >99%), poly(diallyl dimethylammonium (PDDA, 20% wt), rhodamine 6G (99%) and dimethyl methylphosphonate (DMMP, 97%) were purchased from Sigma-Aldrich. All solutions were prepared in distilled water. Acetone and isopropyl alcohol were also purchased from Sigma-Aldrich. DMMP vapours were generated using a calibrated permeation tube (MT-PD-Experimental 107-100-7845-HE3-C50, 126.78 ng/min ± 4.81 ng/min at 80ºC) from VALCO.

### *2.2 Preparation of SERS substrates*

The Ag nanoplates (Ag nPlates) were synthesized according to a previously reported method [13]. Briefly, in a 20 mL vial, the following aqueous solutions were sequentially added while stirring: $H_2O$ (8.5 mL); $AgNO_3$ (3.75 mL, 0.5 mM); sodium citrate (1 mL, 25 mM); $H_2O_2$ (28.2 µL); KBr (10 µL, 1 mM). Finally $NaBH_4$ (1.25 mL, 10 mM) was quickly added to the solution to cause Ag reduction. A colour transition from yellow to blue could be observed in the solution after approximately two minutes, indicating plate formation. Ag nPlates solutions were then centrifuged afterwards for 20 minutes at 21,000 rpm, and the supernatant was centrifuged again. The obtained precipitates were resuspended in water and citrate was added to obtain a solution with a final concentration of 80 mg/L of Ag and 2.5 mM of sodium citrate.

The Ag nPlates were deployed on three different supports (4mm x 8mm): $SiO_2$/Si chip (Sil'Tronix 1 µm of wet thermal $SiO_2$ wafer), stainless steel mesh (see SEM image in Fig. S1) and graphite foil (RivaTherm-HD type from Kempchen). Figure S2 shows digital photographs of the three different supports. Before the deposition the supports were sequentially washed with acetone, isopropanol and water during 10 min each, in an ultrasound bath. After, SERS substrates were immersed in an aqueous solution of PDDA (0.2% v/v) during 4 hours, washed with distilled water and dried for 10 minutes at 100 °C. Finally, the supports were immersed in the Ag nplates suspension overnight and allowed to dry at room temperature, to obtain the SERS substrates. In the case of graphite, before immersing in the PDDA solution the surface was peeled-off with scotch tape. The obtained SERS substrates are denoted as nPlates@$SiO_2$/Si, Ag nPlates@SS and Ag nPlates@graphite for the remainder of this work.

### *2.3 Material Characterization*

Size distribution and morphology of Ag nPlates were studied by TEM (FEI Tecnai T200). Scanning electron microscopy (SEM) images were obtained using a FEG INSPECT 50. Five SEM images of each SERS substrates after coating were analysed to assess the Ag nPlates density on the surface using ImageJ analysis software. A UV-Vis Spectrophotometer Varian Cary 50 Spectrometer was used to measure the absorbance properties of Ag nPlates in solution and Surface Plasmon Resonance (SPR) spectra of the Ag nPlates coated on a glass substrate following the same protocol described above for the other substrates. The measurements of the UV-Vis absorption spectra for the Ag nPlates coated on a stainless steel mesh and graphite substrate were performed in a

Jasco V-670 spectrometer equipped with a diffuse reflectance chamber. The measurements of the solid surfaces were allways obtained with white $BaSO_4$ as reference for the background.

### *2.4 Raman Spectroscopy for characterization of SERS substrates.*

An Alpha 300 Raman spectrometer of WITec was used with a confocal optical microscope (480nm as lateral spatial resolution, 2 $cm^{-1}$ spectral resolution). Raman-SERS spectra were collected in backscattering geometry. Excitation of the samples was carried out with lasers 532nm, 633nm and 785 nm at room temperature and applying a irradiance of 0.13 $mW/\mu m^2$, 0.67 $mW/\mu m^2$ and 0.88 $mW/\mu m^2$, respectively.

The analytical enhancement factor (AEF) [14], of the different substrates, was calculated according to equation (1). R6G was selected as probe molecule monitoring its C-C stretching mode displaced at 1512 $cm^{-1}$.

$$AEF = \frac{\frac{I_{SERS}}{C_{SERS}}}{\frac{I_{Raman}}{C_{Raman}}} \quad (1)$$

Where $C_{Raman}$ and $C_{SERS}$ are the R6G concentration in the Raman measurements and SERS conditions, respectively. And $I_{Raman}$ and $I_{SERS}$ are the normalized intensity values ($cts \cdot mW^{-1} \cdot s^{-1}$) of the 1512 $cm^{-1}$ band for normal Raman and SERS measurements, respectively.

A droplet of 2µL aqueous solution R6G 10 µM was deposited on the SERS substrate and dried under ambient conditions. The R6G spectrum of the SERS substrate was measured in ten different points of the dried droplet and the intensity of the peak at 1512 $cm^{-1}$ was averaged. The normal Raman R6G spectrum was measured focusing the laser beam, 633 nm and 785 nm, in the aqueous solution R6G 1 mM. For the 532 nm laser line, the R6G droplet was dried before acquisition to avoid fluorescence effects.

### *2.5 Experimental set-up for gas phase measurements*

SERS experiments for detecting DMMP in gas phase were conducted in a gas cell ($2.7x10^{-2}$ $cm^3$), where a gas stream, 10ml STP/min, containing 2.5 ppmV (14 $mg/m^3$) of DMMP in nitrogen was fed continuously. DMMP vapours were generated using a calibrated permeation tube as described in our previous work [9]. Two Raman equipments were used: the benchtop equipment described above (Alpha 300 Raman spectrometer, WITec) and a portable Raman BWTEK i-Raman pro system (6 $cm^{-1}$

spectral resolution). In the latter case, an excitation wavelength of 785nm with a power laser of 280 mW (0.035 mW/μm$^2$), 1s of integration time and averaging 100 spectra were used for all the measurements. A schematic drawing together with a picture of the set-up with the portable Raman and the gas cell for measurements are presented in Fig. 1.

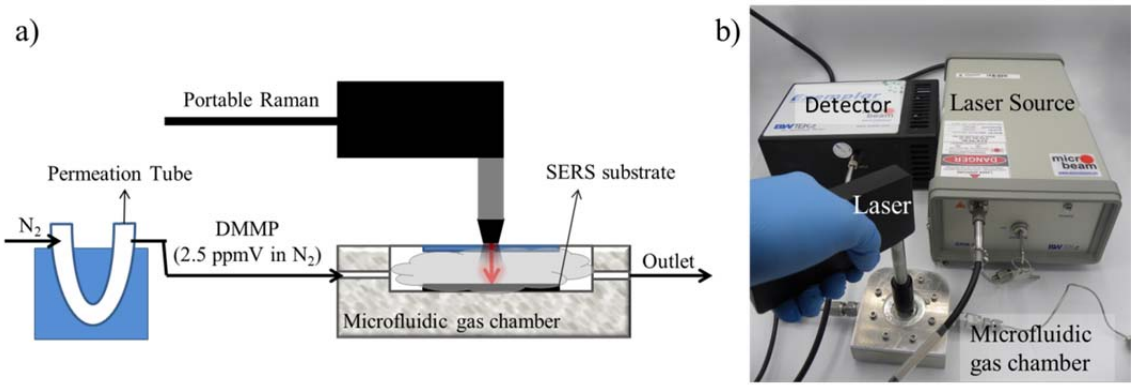


***Fig. 1.*** *a) Scheme of the experimental set-up used for detection of CWA vapours. b) Digital photograph of the real set-up including the portable Raman and the microfluidic gas chamber.*

### *2.6 DFT calculations*

Geometry optimizations and frequency analysis calculations for the organophosphorous compound and Ag atoms were undertaken using DFT methods. All the calculations were carried out using the Gaussian 09 [12] software package.

The ground state geometries were optimized employing the density functional theory (DFT) [15,16] with the B3LYP hybrid functional (Becke's gradient-corrected exchange correlation in conjunction with the Lee–Yang–Parr correlation functional with three parameters) and the 6-311++G(d,p) one-electron atomic basis sets. The adsorbed DMMP molecules and the Ag atoms were calculated with the 6-311++G(d,p) basis set and the LANL2DZ basis set considering a pseudo potential, respectively.

## 3. Results and Discussion

### *3.1 Characterization of SERS substrates*

The synthesis of the Ag nPlates was reproducible and in all the cases the UV-Vis spectrum (Fig. 2a) displayed the main broad band at around 700nm, assigned to the in-plane dipole plasmon resonance. The other two LSPR bands at 460 nm and 331 nm are

assigned to the in-plane quadrupole and out-of-plane quadrupole plasmon resonances of triangular nanoplates, respectively [17]. We observed that during storage at room temperature and in the darkness, the peak intensity progressively decreased and blue shifted to 640 nm after 30 days (see Fig. 2 a). The Localize Surface Plasmon Resonance (LSPR) is very dependent on the shape and size of the nanoparticles, and this evolution is probably caused by surface atomic migration within the Ag nPlate that evolves towards more thermodynamically stable forms [18]. In our case this involves a progressive smoothening of the plates, since the round shape (111), is more stable than tips (110) in triangular shape. The analysis of TEM images for freshly made samples (Fig. 2b) shows a mixture of Ag nanoparticles and nanoplates resulting in an average yield of 85% to plates with an edge of 38 ±15 nm (N>500).

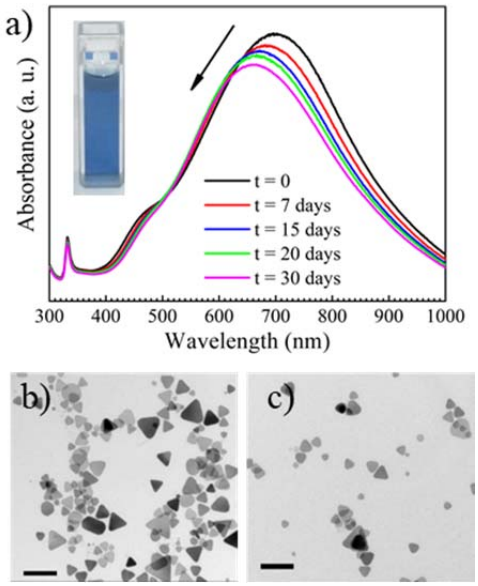


***Fig 2****. a) UV Vis spectra of aqueous solution containing Ag nPlates: evolution with time during storage. Insert: digital photograph of Ag nanoplates solution. TEM image of synthesized Ag plates: b) freshly made and c) aged 30 days. Scale bar 100 nm.*

The SEM images presented in Fig. 3 show a homogeneous distribution of the Ag nPlates deposited on different surfaces. The analysis of the SEM images resulted in a similar surface coverage for the three substrates 42±5% ($SiO_2$/Si chip), 41±5% (stainless steel mesh) and 44±3% (graphite foil) These values are higher than the 30% coverage that we previously found with Au NPs deposited on $SiO_2$/Si surfaces [9]. This could be attributed to the planar structure of the Ag nanoplates, versus the spherical Au nanoparticles. It is also possible to observe densely packed aggregates of nanoplates,

resulting in close contact of their edges that will result in couplings between LSPRs of the metallic nanoplates [19]. The UV-Vis spectrum for the Ag nPlates deposited on the glass substrate broadens and the maximum is blue shifted compared to the nanoplate solution (see Fig. S3). This observation could be attributed to the differences in the dielectric permittivity either of the propagating media of the light, changing from water in the liquid solution to air in the case of the coated substrates [20] or differences in the differences in the properties of underlying substrates [21,22]. The broadening of the spectrum favors the coupling of the plasmon with the different lasers and specially with the 785nm due to the blue shifting observed. In the case of the non-transparent substrates stainless steel and graphite, the diffuse reflectance UV-Vis spectra (Figure S3) showed an increase in the absorption band of the coated substrates in the region above 700nm corresponding to the SPR of the silver plates.

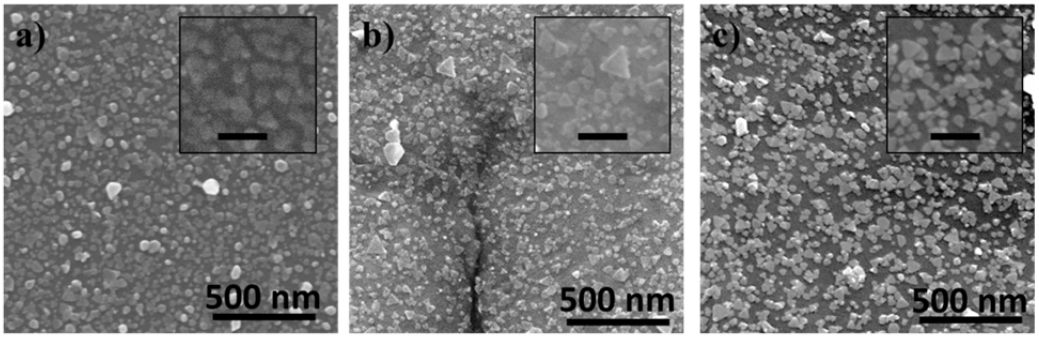


***Fig. 3.*** *SEM images of Ag nanoplates deposited on these SERS substrates: a) $SiO_2$/Si; b) stainless steel mesh; c) graphite foil. Insert scale 50 nm.*

The three substrates were first characterized with R6G as a probe molecule with three different lasers 532, 633 and 785 nm. The as collected spectra, without any modifications (i.e. baseline corrections and smoothing) are presented in Fig. 4. It is immediately apparent that the highest intensity and lower signal to noise ratio for R6G it is observed for the 532 nm laser. The Raman intensity depends on the molecules under study and, when the analyte is a chromophore, close in energy to the frequency of the excitation, resonant Raman scattering (RRS) occurs. The RRS intensities can be $10^6$ larger than normal (off-resonance) Raman intensities [10], in this case we should called the technique SERRS instead of just SERS. When the molecule is adsorbed on the surface of the metal, the strong fluorescence of R6G, is quenched to a certain extent due to non-radiative interactions with the metal surface. When comparing the raw data of the spectra at 532 nm, for the three different substrates (Fig. 4a), the fluorescence of

R6G could observed as a broad band in the spectrum, centered at around 600 $cm^{-1}$. The quenching of this signal is clearly more effective for the case of the graphite substrate. It has been reported that not only graphene, but also other carbonaceous materials could be considered as good SER(R)S substrates due to resonance effect and quenching fluorescence either via charge transfer or energy transfer [23]. In fact, for the $SiO_2$/Si substrate, the one with the lowest conductivity ($10^{-1}$ S/m) we observed the lowest EF and SERS gain (Fig. 4) for all the wavelengths tested.

In the case of the excitation with the 633 nm laser, where the energy of the laser is still near to the excitation of the chromophore, we can still observe the R6G spectra although with lower intensities for the three supports (Fig. 4b). In the case of 785nm laser line, this wavelength matches with the plasmon resonance of the Ag nPlates (see Fig. 2 and Fig. S3), and the spectrum of the R6G molecule could only clearly distinguished for the graphite support (Fig. 4c), most probably due to charge transfer from the electrons of the plasmonic metal to the graphite. The easily available, low cost graphite material could an alternative support for the deposition of active SERS nanostructures being capable of making an additional contribution to the enhancement of the signal by different mechanisms, including fluorescence quenching, charge and energy transfer and also probably resonant effects of this support. This is in accordance with the observations presented by Sil et al. [23] for different carbonaceous materials (charcoal, graphite, MWCNT and GO).

From averaging 10 different spots in each experimental condition (excitation wavelength and substrate), the analytical enhancement factor (AEF) was calculated (Fig. 4d). In the three studied substrates at the excitation wavelength of 785nm reports the highest analytical enhancement factor was obtained, even for the spectra on Ag nPlates@$SiO_2$/Si and Ag nPlates@SS that is less defined. This result is due to the low signal of R6G in Raman conditions ($I_{Raman}$) under excitation wavelength of 785 nm. Fig. S4 shows the Raman spectrum of R6G 1mM under the three excitations wavelength.

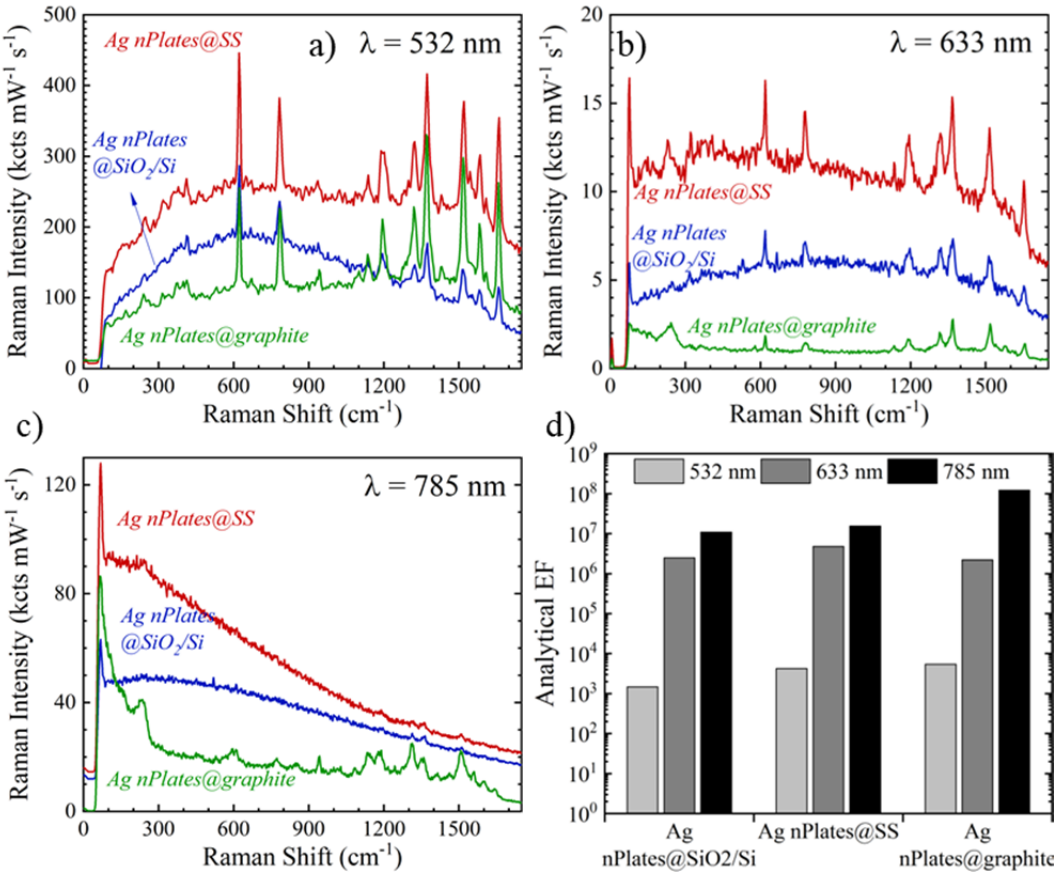


***Fig. 4.*** *Raman spectra of R6G $10^{-5}$M droplet dried on three different SERS substrates: Ag nPlates@$SiO_2$/Si, Ag nPlates@SS and Ag nPlates@graphite for different excitation wavelengths: a) 532 nm: b) 633 nm and c) 785nm. d) Analytical EF (AEF) calculated for the three SERS substrates and for different excitation wavelengths (532, 633 and 785 nm). For better visualization in a) and c) spectra have been vertically translated.*

### *3.2 CWAs gas phase detection capabilities of the SERS substrates*

The SERS substrates were also tested for the measurement of the simulant nerve agent DMMP in gas phase in the benchtop equipment using the 785nm laser and graphite substrate, which resulted in the highest AEF. Furthermore in the case of using 633nm and 785nm with $SiO_2$/Si and stainless steel mesh substrates, it was not possible to get a spectrum. As soon as the laser was focused on the sample, the DMMP molecules were decomposed and a broad band in the region 1450 to 1700 $cm^{-1}$, corresponding to amorphous carbon was observed. This phenomenon is attributed to the photo-thermal decomposition of the DMMP molecules adsorbed on the enhancing metal surface [24].

306 The Raman spectrum for neat liquid DMMP and the SERS spectra on Ag
307 nPlates@graphite for a concentration of 2.5ppmV DMMP in the gas phase are
308 presented in Fig. 5a and Fig 5b for benchtop and portable Raman equipments,
309 respectively. First of all, it is important to note that the fingerprint of the DMMP
310 molecule is observed with both detectors. However the relative intensity of the
311 characteristic bands differs from the acquired at normal Raman conditions. The Raman
312 spectra recorded by the portable equipment on randomly selected spots are presented in
313 Fig. 5b. Due to the lower resolution of the portable equipment, 6 $cm^{-1}$, compared to 2
314 $cm^{-1}$ in the benchtop equipment, the bands are broader and could be also slightly
315 shifted. This is clearly observed for the main band of the DMMP liquid measured in
316 both equipments. It is important to note that the spectra were reproducible in all the
317 randomly selected spots, showing three distinctive bands, with similar intensities and
318 assigned to $PO_3$, P-C stretching and $PO_2$ bending (for more details see Table 1). This
319 allowed a clear identification of the DMMP using the hand held instruments, for a gas
320 phase concentration of 2.5 ppmV.

321 Fig. 6a shows the molecular structures of the two investigated DMMP-Ag
322 complexes. The most stable Ag-DMMP geometry, among studied, corresponds with
323 DMMP molecule adsorbed on 6 Ag atoms (in blue) though P=O group. A less-stable
324 Ag-DMMP* complex resulting from DMMP approximation of the phosphate group that
325 looks like an umbrella, $(PO_3)_{umbrella}$ is also plotted.

326 Fig. 6b compiles the simulated Raman spectra of DMMP molecule and DMMP-Ag
327 complexes. Comparing with the most significant bands from experimental SERS spectra
328 (see Fig. 5 and Table 1), simulated Raman spectra show similar bands, although
329 changes in both relative intensities and the position of the bands are clearly noticed.
330 Bands at 504 and 715 $cm^{-1}$ assigned to $(PO_3)_{umbrella}$ bending and to $(P–CH_3)$ stretching +
331 (P–O) stretching + $(P–O–CH_3)$ bending, respectively, are slightly displaced to around
332 483 and 672 $cm^{-1}$ (for more details see Table 1). The ratio between these two simulated
333 bands (Intensity at 672 $cm^{-1}$ / Intensity at 483 $cm^{-1}$) for DMMP molecule and Ag-
334 DMMP (P=O) complex is the same. However, the simulated spectrum for Ag-DMMP*
335 ($PO_3$) shows an increment in this ratio, similar to the one observed experimentally. This
336 could provide some insight on the adsorption dynamics of DMMP molecules on Ag
337 plates under experimental conditions. Although less energetically favored, this
338 geometry is contributing to the dynamic SERS response. However, it should be noticed

that for simplicity the simulation considers one DMMP molecule and 6 silver atoms while experimentally, a molecule of DMMP may interact not only with several silver atoms but also with other DMMP molecules, increasing the possibilities of $(PO_3)_{umbrella}$ – Ag interactions.

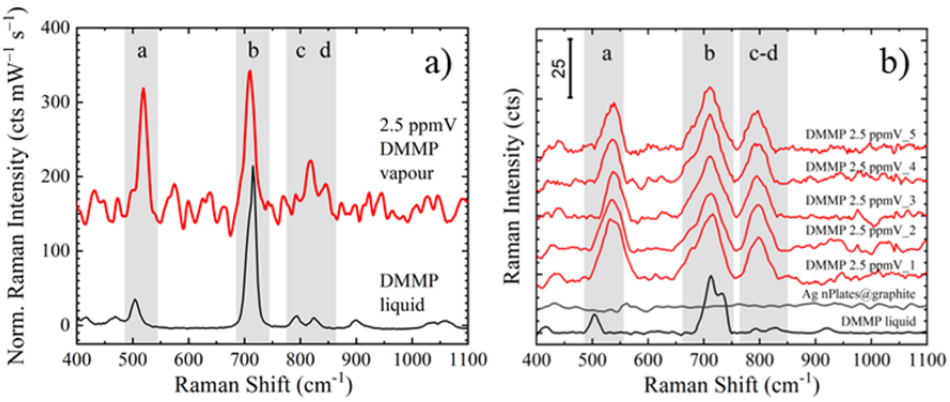


***Fig 5.*** *Raman spectra of DMMP liquid and DMMP in vapour phase (2.5 ppmV, 14 mg/m$^3$) measured on Ag nplates@graphite using: a) the benchtop equipment and b) the portable equipment. For the portable equipment five different spectra for vapours detection are shown, measured at different random spots on the support, together with the spectrum of Ag nPlates@graphite. (a-b) Excitation wavelength 785 nm; grey shadows indicate bands assigned to DMMP (more information in Table 1).*

***Table 1.*** *Temptative assignments of the experimental Raman and SERS bands for DMMP pure liquid and vapor on Ag nPlates@graphite, together with calculated values by DFT simulations.*

| Band | Raman Shift of DMMP vibrational modes (cm$^{-1}$) | | | | | Temptative assignment [25] |
|---|---|---|---|---|---|---|
| | Pure liquid Experimental | Calculated DMMP in vacuum | DMMP Vapors on Ag nPlates@graphite: Benchtop equipment | DMMP Vapors on Ag nPlates@graphite: Portable equipment | Calculated Ag- DMMP ($PO_3$) | |
| a | 504 | 483 | 515 | 539 | 469 | Bending $PO_3$ |
| b | 715 | 672 | 710 | 712 | 663 | Stretching PC |
| c | 794 | 756 | 814 | 797 | 756 (weak) | Bending $PO_2$ |
| d | 825 | 791 | 845 | (broad) | 785 | Bending $PO_2$ |

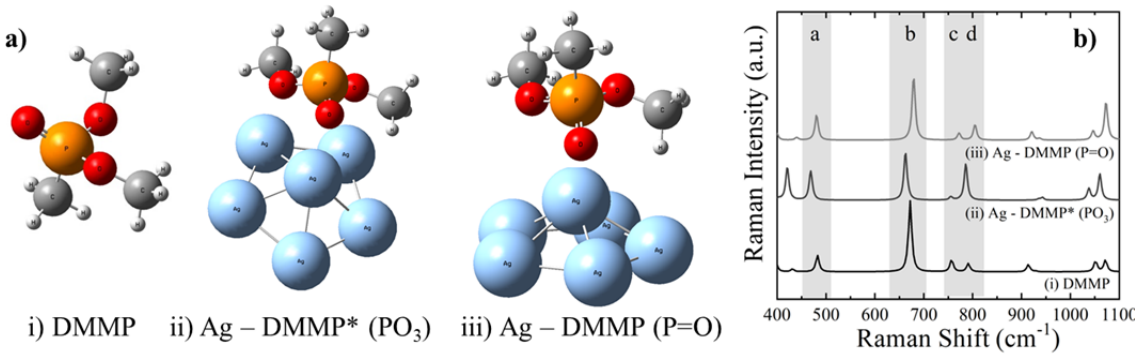


353

354 ***Fig. 6.*** *a) Optimized geometries for the DMMP in vacuum (i) and absorbed on six Ag atoms*
355 *according to the following possibilities: (ii) anchoring through the three oxygen atoms*
356 *of DMMP ($PO_3$) and (iii) interaction via P=O group. b) Calculated spectra of DMMP*
357 *(i) and DMMP-Ag complexes considering de adsorption of DMMP on three silver*
358 *atoms through: (ii) the three oxygens ($PO_3$) and (iii) P=O group. Grey shadows*
359 *indicate bands assigned to DMMP (more information in Table 1).*

360 To evaluate the reproducibility of the Ag nplates@graphite fabrication method,
361 three different Ag nplates@graphite substrates were prepared, and the SERS spectra
362 (2.5ppmV DMMP) were collected randomly in ten different spots. Figure 7a shows the
363 average peak intensity at 712 $cm^{-1}$ of DMMP, showing an average relative standard
364 deviation (RSD) for the SERS intensity of 5%. This value indicates the good
365 reproducibility of fabrication method and also the detection capabilities of Ag
366 nPlates@graphite substrates.

367 Finally, we further evaluate the concept of SERS sensor for rapid CWAs detection
368 in gas phase. Figure 7b shows the intensity evolution of DMMP, monitoring peak
369 displayed at 712 $cm^{-1}$, as a function of exposure time to the vapours of this gas. It is
370 important to note that the response time $t_{50\%}$ defined as the time to reach 50% or 90% of
371 the final Raman intensity, is $t_{50\%}$ =137s and $t_{90\%}$ is only 261s. This value is outstanding
372 compared to the early work for detection of DMMP in gas phase that needed 40 minutes
373 exposure to acquire a meaningful spectrum with the benchtop equipment available at
374 that time. This time is slightly higher than the response time that we found in our
375 previous study with benchtop equipment [9]. It is also important to note that due to the
376 lower resolution of the handheld equipment, the acquisition time is higher (100s)
377 compared to (1s) in benchtop equipment. Although it is difficult to compare detection
378 values for different conditions, molecules and equipment's, the relevance of the
379 obtained results it is presented in Table 2 with the available literature data for gas phase

detection at concentrations below 10 ppm. These results demonstrate the high quality of Ag nplates@graphite as SERS sensors of gas molecules, combined with handheld equipment for real applications on field.

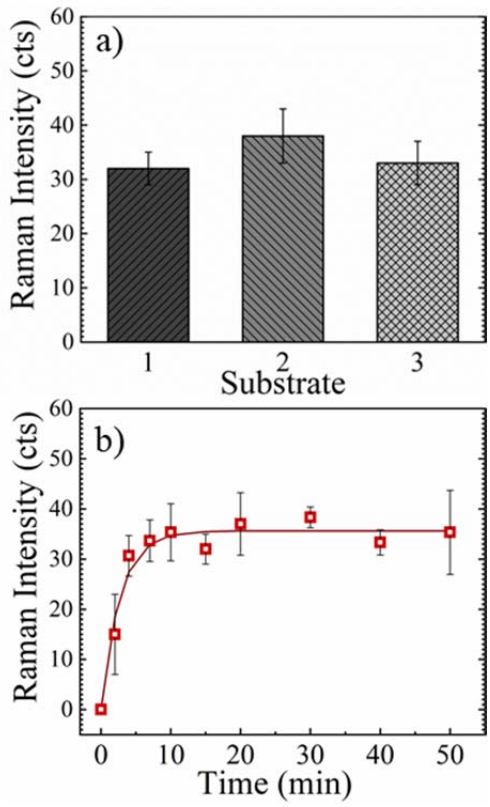


***Fig. 7.*** *a) The reproducibility of the Ag nplates@graphite: average intensity of the peak at 712 $cm^{-1}$ of DMMP (2.5 ppmV) of three different Ag nplates@graphite. The error bars indicate standard deviation. b) Intensity value of the peak at 712 $cm^{-1}$ of DMMP as a function of exposure time to 2.5 ppmV. Both experiments were carried out with the portable Raman equipment.*

***Table 2.*** *Literature review for gas phase detection of different molecules, at concentrations below 10ppm, with SERS as detection technology.*

| Material | Target molecule | Raman equipment | Limit of detection | Detection time | Ref. |
|---|---|---|---|---|---|
| Ag nPlates@graphite | DMMP | Portable | 2.5 ppmV | 137 s | This work |
| Cool Ag nanorods | Benzene | Portable | 10 ppmV | 2 min | [7] |
| Ag@silica nanospheres | Benzene thiol (BT) | Portable | 8 ppmV | 50-100 s | [2] |
| Au-Ag nanowires | $NO_2$ | Portable | 100 ppbV | 3 min | [8] |
| Agnanorods@$HfO_2$ | 2-naphtalenethiol | Portable | 20 ppbV | 40 min | [3] |
| Gold nanopillars | Hydrogen cyanine | Benchtop | 5 ppmV | 15 min | [5] |
| AuNP@citrate | DMMP | Benchtop | 625 ppbV | 120s | [9] |
| Agnanocubes@ZIF8 | 2-nitrotoluene | Benchtop | 50 ppbV | 15 min | [6] |

## 4. Conclusions

The effect of different substrates ($SiO_2$/Si, stainless steel mesh and graphite foil), where plasmonic silver nanoplates were deposited, on the SERS signal, with three lasers ($\lambda$=532, 633 and 785nm) has been evaluated with two molecules R6G in liquid and DMMP, 2.5ppmV in gas phase. It has been demonstrated that graphite is the best choice because of efficient quenching of the fluorescent signal ($\lambda$=532 and 633nm), via charge transfer or energy transfer. This energy transfer is also important when working with the 785nm laser line, with its wavelength matching the plasmon resonance of the silver nanoplates. In this case a clear spectrum of R6G could be only distinguished on graphite support. When working with DMMP, it was only possible to use the 785nm laser in combination with graphite, otherwise the high energy concentrated on the sample during measurement decomposed the adsorbed DMMP molecules. The interactions of the DMMP molecule with the silver surface modify the intensities and positions of the vibrational Raman bands. DFT simulations suggest such variations by the formation of Ag-DMMP complexes via the $PO_3$ umbrella. The SERS measurements carried out in different prepared samples with the handheld Raman equipment for 2.5 ppmV in gas phase showed a fast response and reproducible fingerprint of the molecule and relative

standard deviation of SERS intensity signal of 5%, paving the way for on field applications.

## Conflict of interest:

Authors declare that there are no conflicts of interest.

## Acknowledgements

Authors are grateful for financial support from the European Union's Horizon 2020 research and innovation programme under the Marie Sklodowska-Curie grant agreement Nr. 823895, MICINN (CTQ2013-49068-C2-1-R and CTQ2016-79419-R), Gobierno de Aragón (T57-17R p), Feder 2014-2020 "Construyendo Europa desde Aragón") and CIBER-BNN (initiative funded by the VI National R&D&i Plan 2008–2011, Iniciativa Ingenio 2010, Consolider Program, CIBER Actions and financed by the Instituto de Salud Carlos III with assistance from the European Regional Development Fund). Authors would like to acknowledge the use of Servicio General de Apoyo a la Investigación-SAI, Universidad de Zaragoza. The microcopy works have been conducted in the Laboratorio de Microscopias Avanzadas at Instituto de Nanociencia de Aragon-Universidad de Zaragoza. Authors acknowledge the LMA-INA for offering access to their instruments and expertise.

## References

[1] A. Hakonen, P.O. Andersson, M. Stenbæk Schmidt, T. Rindzevicius, M. Käll, Explosive and chemical threat detection by surface-enhanced Raman scattering: A review, Anal. Chim. Acta. 893 (2015) 1–13. doi:10.1016/j.aca.2015.04.010.

[2] K.B. Biggs, J.P. Camden, J.N. Anker, R.P.V. Duyne, Surface-enhanced raman spectroscopy of benzenethiol adsorbed from the gas phase onto silver film over nanosphere surfaces: Determination of the sticking probability and detection limit time, J. Phys. Chem. A. 113 (2009) 4581–4586. doi:10.1021/jp8112649.

[3] L. Ma, H. Wu, Y. Huang, S. Zou, J. Li, Z. Zhang, High-Performance Real-Time SERS Detection with Recyclable Ag Nanorods@HfO2 Substrates, ACS Appl. Mater. Interfaces. 8 (2016) 27162–27168. doi:10.1021/acsami.6b10818.

[4] R.K. Lauridsen, T. Rindzevicius, S. Molin, H.K. Johansen, R.W. Berg, T.S.

445 Alstrøm, K. Almdal, F. Larsen, M.S. Schmidt, A. Boisen, Towards quantitative
446 SERS detection of hydrogen cyanide at ppb level for human breath analysis,
447 Sens. Bio-Sensing Res. 5 (2015) 84–89. doi:10.1016/j.sbsr.2015.07.002.

448 [5] R.K. Lauridsen, P.B. Skou, T. Rindzevicius, K. Wu, S. Molin, S.B. Engelsen,
449 K.G. Nielsen, H.K. Johansen, A. Boisen, SERS spectroscopy for detection of
450 hydrogen cyanide in breath from children colonised with: P. aeruginosa, Anal.
451 Methods. 9 (2017) 5757–5762. doi:10.1039/c7ay01693j.

452 [6] C.S.L. Koh, H.K. Lee, X. Han, H.Y.F. Sim, X.Y. Ling, Plasmonic nose:
453 Integrating the MOF-enabled molecular preconcentration effect with a plasmonic
454 array for recognition of molecular-level volatile organic compounds, Chem.
455 Commun. 54 (2018) 2546–2549. doi:10.1039/c8cc00564h.

456 [7] M.K. Oh, R. De, S.Y. Yim, Highly sensitive VOC gas sensor employing deep
457 cooling of SERS film, J. Raman Spectrosc. 49 (2018) 800–809.
458 doi:10.1002/jrs.5355.

459 [8] S. Kim, D.H. Kim, S.G. Park, Highly sensitive and on-site NO 2 SERS sensors
460 operated under ambient conditions, Analyst. 143 (2018) 3006–3010.
461 doi:10.1039/c8an00845k.

462 [9] M. Lafuente, I. Pellejero, V. Sebastián, M.A. Urbiztondo, R. Mallada, M.P. Pina,
463 J. Santamaría, Highly sensitive SERS quantification of organophosphorous
464 chemical warfare agents: A major step towards the real time sensing in the gas
465 phase, Sensors Actuators, B Chem. 267 (2018). doi:10.1016/j.snb.2018.04.058.

466 [10] E. Le Ru, P.G. Etchegoin, Principles of Surface-Enhanced Raman Spectroscopy:
467 and related plasmonic effects., Elsevier, 2009.

468 [11] N. Taranenko, J.-P. Alarie, D.L. Stokes, T. Vo-Dinh, Surface-Enhanced Raman
469 Detection of Nerve Agent Simulant (DMMP and DIMP) Vapor on
470 Electrochemically Prepared Silver Oxide Substrates, J. Raman Spectrosc. 27
471 (1996) 379–384. doi:10.1002/(SICI)1097-4555(199605)27:5<379::AID-
472 JRS925>3.0.CO;2-G.

473 [12] M.J. Frisch, G.W. Trucks, H.B. Schlegel, G.E. Scuseria, M.A. Robb, J.R.
474 Cheeseman, G. Scalmani, V. Barone, B. Mennucci, G.A. Petersson, Gaussian 09,

475 Revision D. 01, 2013, Gaussian, Inc., Wallingford CT. (2013).

476 [13] A.J. Frank, N. Cathcart, K.E. Maly, V. Kitaev, Synthesis of silver nanoprisms
477 with variable size and investigation of their optical properties: A first-year
478 undergraduate experiment exploring plasmonic nanoparticles, J. Chem. Educ. 87
479 (2010) 1098–1101. doi:10.1021/ed100166g.

480 [14] E.C. Le Ru, E. Blackie, M. Meyer, P.G. Etchegoint, Surface enhanced raman
481 scattering enhancement factors: A comprehensive study, J. Phys. Chem. C. 111
482 (2007) 13794–13803. doi:10.1021/jp0687908.

483 [15] A.D. Becke, Density-functional thermochemistry. III. The role of exact
484 exchange, J. Chem. Phys. 98 (1993) 5648–5652. doi:10.1063/1.464913.

485 [16] P.J. Stephens, F.J. Devlin, C.F. Chabalowski, M.J. Frisch, Ab Initio calculation
486 of vibrational absorption and circular dichroism spectra using density functional
487 force fields, J. Phys. Chem. 98 (1994) 11623–11627. doi:10.1021/j100096a001.

488 [17] H. Hou, P. Wang, J. Zhang, C. Li, Y. Jin, Graphene Oxide-Supported Ag
489 Nanoplates as LSPR Tunable and Reproducible Substrates for SERS
490 Applications with Optimized Sensitivity, ACS Appl. Mater. Interfaces. 7 (2015)
491 18038–18045. doi:10.1021/acsami.5b04946.

492 [18] X. Jiang, Q. Zeng, A. Yu, Thiol-frozen shape evolution of triangular silver
493 nanoplates, Langmuir. 23 (2007) 2218–2223. doi:10.1021/la062797z.

494 [19] J. Lee, B. Hua, S. Park, M. Ha, Y. Lee, Z. Fan, H. Ko, Tailoring surface
495 plasmons of high-density gold nanostar assemblies on metal films for surface-
496 enhanced Raman spectroscopy, Nanoscale. 6 (2014) 616–623.
497 doi:10.1039/c3nr04752k.

498 [20] S.K. Ghosh, S. Nath, S. Kundu, K. Esumi, T. Pal, Solvent and ligand effects on
499 the localized surface plasmon resonance (LSPR) of gold colloids, J. Phys. Chem.
500 B. 108 (2004) 13963–13971. doi:10.1021/jp047021q.

501 [21] F.J. Beck, E. Verhagen, S. Mokkapati, A. Polman, K.R. Catchpole, Resonant SPP
502 modes supported by discrete metal nanoparticles on high-index substrates, Opt.
503 Express. 19 (2011) A146. doi:10.1364/oe.19.00a146.

[22] M.W. Knight, Y. Wu, J.B. Lassiter, P. Nordlander, N.J. Halas, Substrates matter: influence of an adjacent dielectric on an individual plasmonic nanoparticle, Nano Lett. 9 (2009) 2188–2192. doi:10.1021/nl900945q.

[23] S. Sil, N. Kuhar, S. Acharya, S. Umapathy, Is chemically synthesized graphene "Really" a unique substrate for SERS and Fluorescence quenching?, Sci. Rep. 3 (2013) 1–6. doi:10.1038/srep03336.

[24] M. Lafuente, E.J.W. Berenschot, R.M. Tiggelaar, R. Mallada, N.R. Tas, M.P. Pina, 3D fractals as SERS active platforms: Preparation and evaluation for gas phase detection of G-nerve agents, Micromachines. 9 (2018). doi:10.3390/mi9020060.

[25] J.C.S. Costa, R.A. Ando, A.C. Sant'Ana, P. Corio, Surface-enhanced Raman spectroscopy studies of organophosphorous model molecules and pesticides, Phys. Chem. Chem. Phys. 14 (2012) 15645–15651. doi:10.1039/c2cp42496g.

# Supporting Information

# Gas phase detection of Chemical Warfare Agents

# CWAs with portable Raman

Marta Lafuente [a,b], Diego Sanz [a,b], Miguel Urbiztondo [c], Jesús Santamaria [a,b,d], María Pilar Pina [a,b,d], Reyes Mallada[a,b,d,*]

[a]*Nanoscience Institute of Aragon (INA), University of Zaragoza, Department of Chemical & Environmental Engineering, Edificio I+D+i, Campus Rio Ebro, C/Mariano Esquillor s/n, 50018 Zaragoza, Spain*

[b]*Instituto de Ciencia de Materiales de Aragón (ICMA), Universidad de Zaragoza-CSIC, 50009 Zaragoza, Spain.*

[c]*Centro Universitario de la Defensa de Zaragoza, Carretera Huesca s/n, 50090 Zaragoza, Spain.*

[d]*Networking Research Center on Bioengineering, Biomaterials and Nanomedicine, CIBER-BBN, 28029 Madrid, Spain.*

**Figure S1.**

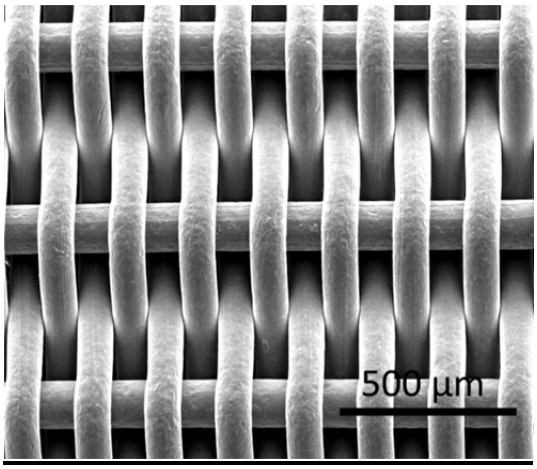


**Figure S1**. SEM image of the stainless steel mesh used as SERS substrate support.

**Figure S2.**


**Figure S2**. Digital photographs of the three different supports used as SERS substrate: a) $SiO_2$/Si chip; b) stainless steel mesh and c) graphite foil. Rule in centimeters (cm).

**Figure S3.**

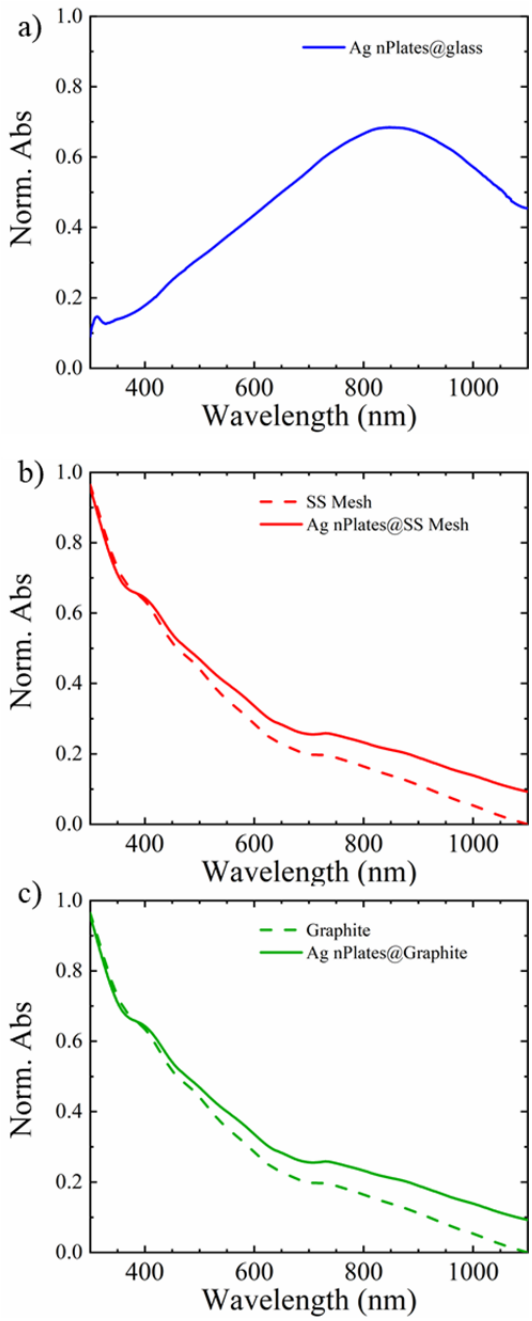


**Figure S3**. UV-Vis spectra of deposited Ag nanoplates on (a) glass; (b) Ag nPlates@SS Mesh and (c) graphite. The spectra of mesh and graphite before incorporating Ag nPlates are also plotted.

**Figure S4**.

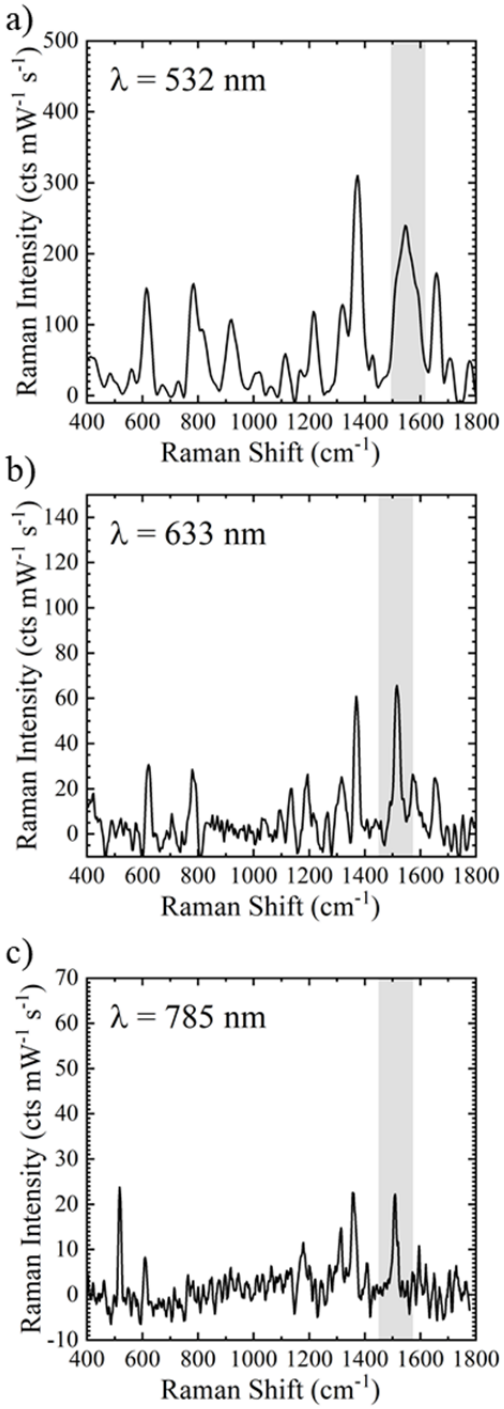


***Figure S4****. Raman spectra of Rhodamine 6G (R6G, 1mM) measured under the three different excitation wavelengths: a) 532nm; b) 633nm and c) 785nm. Grey shadow indicates vibrational mode selected for AEF calculations: PC stretching around 1512 cm$^{-1}$.*